Accepted Manuscript

Microwave-assisted synthesis and characterization of WO_X nanostructures for gas sensor application

K. Movlaee, P. Periasamy, T. Krishnakumar, M.R. Ganjali, S.G. Leonardi, G. Neri, Murthy Chavali, Prem Felix Siril, V.P. Devarajan

PII: S0925-8388(18)31902-9

DOI: 10.1016/j.jallcom.2018.05.189

Reference: JALCOM 46165

To appear in: *Journal of Alloys and Compounds*

Received Date: 5 March 2018

Revised Date: 14 May 2018

Accepted Date: 16 May 2018

Please cite this article as: K. Movlaee, P. Periasamy, T. Krishnakumar, M.R. Ganjali, S.G. Leonardi, G. Neri, M. Chavali, P.F. Siril, V.P. Devarajan, Microwave-assisted synthesis and characterization of WO_X nanostructures for gas sensor application, *Journal of Alloys and Compounds* (2018), doi: 10.1016/j.jallcom.2018.05.189.

Microwave-assisted synthesis and characterization of WO_x nanostructures for gas sensor application

Movlaee K[1,2], Periasamy P[3], Krishnakumar T[4], Ganjali MR[2], Leonardi SG[1], Neri G[1], Murthy Chavali[5], Prem Felix Siril[6], Devarajan V.P[7]

[1]Department of Engineering, University of Messina, 98166 Messina, Italy

[2] Center of Excellence in Electrochemistry, School of Chemistry, College of Science, University of Tehran, Iran

[3] Excel college of Engineering and Technology, Komarapalayam, Namakkal – 637 303, Tamilnadu, India

[4] Tagore Institute of Engineering and Technology, Attur, Salem – 636 112, Tamilnadu, India.

[5]Analytical chemistry & Nanotechnology, VFSTRA University, Guntur – 522 213, Andhra Pradesh, India

[6] School of Basic Sciences, Indian Institute of Technology, Mandi, Mandi – 175 001, India

[7] KSR Arts College for Women, Tiruchengode, Namakkal – 637 214, Tamilnadu, India

Abstract

Tungsten oxide (WO_x) nanoparticles were synthesized by a facile and eco-friendly microwave-assisted hydrothermal method without need for using any surfactant. A thorough investigation was performed in order to elucidate the effects of microwave irradiation time (10, 20 and 30 minutes) on the structural, morphological and optical properties of the as-prepared WO_x. Scanning electron microscopy (SEM) and high-resolution transmission electron microscopy (HRTEM) of the samples revealed the presence of irregular nanosized particles containing some well-structured rod shape particles. Fourier transform infrared spectroscopy (FTIR) and X-ray diffraction (XRD) indicated that these nanoparticles are crystallines with mean crystalline size of about 16 nm exhibiting both monoclinic and orthorhombic WO_x crystal structures. The optical properties were investigated by using ultraviolet visible spectroscopy (UV-VIS) and photoluminescence (PL). A blue-shifted optical absorption spectrum with an enhanced defects emission was observed when it was compared to bulk spectrum of WO_3. Thermal-aged WO_x nanoparticles at mild temperature (350 °C) were also used to fabricate conductometric gas sensors Gas sensing tests showed excellent performance towards ethanol monitoring for each synthesized material. In particular, the highest sensitivity was obtained for the sensor based on WO_x synthesized by 10 minutes irradiation time (S10). At the optimal operating temperature of 300 °C, the S10 sensor showed a response R_a/R_g = 8.5 towards 100 ppm ethanol with fast response time of 10 s, in addition to an excellent selectivity against common interfering gases.

Keywords: *Tungsten Oxide, Microwave irradiation, Nanostructures, Gas sensor, Ethanol.*

1. Introduction

In the past decades, metal oxide nanostructures have been largely investigated thanks to their potential performances for many applications. Among these, it is well known that tungsten oxide (WO_3) nanomaterials provide superior electrical properties compared to those of bulk materials. WO_3 is an n-type semiconductor material with narrow bandgap (~2.7 eV) which shows flexible physical and chemical properties, thus it has found various applications in different fields such as electro-chromic window [1, 2], gas sensor [3], optical device [4], supercapacitors [5], solar energy devices [6] and (photo)catalysts [7, 8].

Several methods have been developed for the preparation of WO_3 and their non-stoichiometric WO_x nanostructures including sol-gel [9], electro-spinning [10], micro-emulsion [11], acid precipitation [12] and ion-exchange [13]. On the other hand, modification of the size and morphology of the obtained nanostructures has been one of the most challenging issues in fundamental scientific interest and technological applications. In this respect, microwave assisted hydrothermal method has drawn much attention of researchers owing to its easy way of synthesis, controlling over morphology, cost/energy saving and being fast for synthesizing metal oxides [14].

Previous papers on the microwave-assisted hydrothermal synthesis generally report the use of additive/surfactant(s) to tailor the morphology of the WO_3 nanoparticles. As an example, Sun et al. [15] described the preparation of monodisperse $WO_3 \times 2H_2O$ nanospheres with L (+) tartaric acid as a protective agent. Le Houx et al. [16] prepared WO_3 nanoparticles using benzyl alcohol as additive. Sungpanich et al. [17] synthesized WO_3 nanoplates using citric acid as additive. Phuruangrat et al. [18] synthesized uniform WO_3 nanowires by a microwave-assisted hydrothermal process in a solution containing $(NH_4)_2SO_4$ as a capping at 150 °C for 3 h. Only very few researchers reported additive-, template- or surfactant-free chemical routes assisted by microwave for synthesizing WO_3. Hernandez-Uresti et al. [19]

synthesized WO_3 nanoparticles via in 30 or 60 min microwave-assisted hydrothermal process without the use of any additives, followed by thermal treatments at high temperature as 700 °C. Le Houx et al. [20] prepared WO_3 nanoparticles by solvothermal treatment of tungsten chloride in benzyl alcohol up to 210 °C followed by annealing in air at 350 °C. Chang et al. prepared crystalline tungsten oxide mixtures, WO_3–$WO_3 \cdot 0.5H_2O$, by microwave-assisted hydrothermal synthesis at 180 °C for 45 min [21].

In this study, we have synthesized WO_x nanostructures with the help of microwave irradiation using different irradiation time intervals without using any additive, obtaining crystalline phases just after 10 min of microwave irradiation. The structural, morphological and optical properties were investigated and discussed. WO_x nanostructures display also high potential for gas sensing in the ppm range [22-24]. Few papers can be instead found in literature on conductometric sensors based on pure WO_3 for detecting ethanol [25- 27]. Ethanol is one of the most common chemicals and has many applications in food, biomedical, transportation, and chemical industries, thus its quantitative monitoring at ppm levels is of outmost importance [28]. Therefore, the sensing properties of as synthesized WO_x nanoparticles, after a proper thermal-aging, were investigated in order to assess their sensing properties toward ethanol monitoring in air.

2. Experimental

2.1. Materials

All the chemicals used were of analytical grade and used without any further treatment such as sodium tungstate (Na_2WO_4), hydrochloric acid (HCl) and distilled water as the solvent.

2.2. Synthesis of WO_x nanoparticles

For the synthesis of WO_x nanoparticles, 0.1 mole of Na_2WO_4 was dissolved in 100 ml distilled water. After that, 6 ml HCl solution was added dropwise to adjust the pH at about 1-

2. After this addition, the solution color changed, from transparent into the pale-yellow color. The solution was kept at rest to form the precipitate. Afterward, the precipitation was carefully collected and washed with distilled water several times and placed in a microwave oven for microwave irradiation using different time intervals, i.e. 10, 20 and 30 min. The microwave irradiated samples was allowed to dry using hot plate for 30 min. The final product was then heated at 120 °C for 5 hours using muffle furnace to remove the water content. Hereafter, we assigned the code S10, S20 and S30 to samples obtained under the different irradiation time. Finally, a part of these samples was also thermal-aged in air at the temperature of 350 °C for 2 hours.

2.3. Characterization

The powder samples were used for various characterization techniques to evaluate their structural, morphology and optical properties. The crystal structure was confirmed using X-ray diffraction technique (XRD, model: PANalytical X'pert Pro). The chemical structure and functional groups were studied using Fourier transform infrared spectroscopy (FTIR, model: Jasco-6300). The surface morphology was observed using scanning electron microscope (SEM model: Vega 3 Sbh Tescan Brno S.R.O) and the surface morphology as well as particle distribution were observed using high resolution transmission electron microscope (HRTEM, model: FEI USA, FP-5022). The elemental composition was assessed using energy dispersive X-ray spectroscopy analysis (EDAX, model: EDAX-EDS-SSD). The optical absorption behaviors were investigated using ultra-violet visible spectroscopy technique (UV-Vis, model: Agilent-8453). Photoluminescence spectroscopy technique (PL, model: Agilent) was applied to investigate the emission behavior of samples.

2.4 Electrical and sensing test

Sensors were made by printing films (around 10-30 μm thick) of paste of the nano-powders dispersed in water on alumina substrates (6×3 mm^2) with Pt interdigitated electrodes and a Pt heater located on the backside. Sensors were introduced in a stainless-steel test chamber for the sensing tests. The experimental bench for the electrical characterization of

the sensors, allows to carry out measurements in controlled atmosphere. Preliminary tests were carried out in order to evaluate the electrical resistance of the sensor by increasing the temperature from 25 to 100 °C, with step of 8 °C/min, under 100 cc/min dry air flow. Electrical sensing tests were carried out in the temperature range from room temperature (25 °C) to 350 °C, with steps of 25 °C, under a dry air total stream of 100 sccm, collecting the sensors resistance data in the four point mode. Gases coming from certified bottles can be further diluted in air at a given concentration by mass flow controllers. A multimeter data acquisition unit Agilent 34970A was used for this purpose, while a dual-channel power supplier instrument Agilent E3632A was employed to bias the built-in heater of the sensor to perform measurements at super-ambient temperatures. The gas response, S, is defined as:

$$S = R_{air}/R_g \quad (1)$$

where R represents the electrical resistance of the sensor at different ethanol concentrations and R_{air} the baseline resistance in dry air. Response and recovery times were calculated at 90% of signal variation after exposure to ethanol and dry air, respectively.

3. Result and Discussion

3.1. Morphological and structural analysis of as-synthetized samples

A detailed characterization was first carried out to understand the morphological and microstructural characteristics of the as-synthesized samples. **Figure 1** shows SEM images of samples synthesized varying the microwave irradiation time. All samples appears to be highly agglomerated forming large grains having size in the range of micrometer. These large agglomerated are composed of smaller particles, as documented by high magnification images shown in the inset.

Elementary analysis was undertaken to ascertain the presence of impurity or foreign elements. EDAX spectra reported in **Figure 2**, show W and O as the main elements, highlighting the good purity of the synthesized nanopowders.

Due to the small dimension of primary particles and their extensive agglomeration, no clear information can be obtained about their shape/morphology through SEM analysis. Therefore, a TEM investigation was performed to reveal the shape/morphology of the WO_x grains (**Figure 3).** TEM images in **Figure 3a-c** show that the particles of the as-synthesized samples have irregular shape and their size are in the nanometer range. It was also noted the presence of some well-structured rod shape particles. HRTEM image of one of this rod-like particle for the S30 sample, having dimensions of more or less 35 × 15 nm, is reported in **Figure 3d**. The value of interlayer spacing (d) was measured as 3.8 Å, which corresponds well to (002) planes of WO_3 crystalline phase.

XRD patterns of the as-prepared samples evidenced the formation of WO_x crystalline nanostructures within 10 minutes without post-synthesis heating **(Figure 4)**. In particular, these patterns are characterized by the presence of reflection peaks indexed to $WO_{2.90}$ monoclinic and β-WO_3 orthorhombic crystal structures. Miller indices values were in good agreement with the standard values reported in the JCPDS card No. 36-0102 and 89-4479, respectively. Orthorhombic structure was dominant with corresponding planes of (002), (012), (212) and (312). In addition, monoclinic structure was also identified with corresponding planes of (111), (115), (020) and (032). It is noteworthy that, increasing the microwave irradiation time, $WO_{2.90}$ monoclinic phase appears to transform into β-WO_3 orthorhombic phase.

The large peak broadening confirms the formation of nano-sized structures. The crystallite sizes were calculated using Scherrer's formula from high intense (111) plane and calculated sizes were in the range 14-18 nm.

Figure 5 shows the FTIR spectra of as obtained microwave irradiated samples. The observed transmittance peaks match well with other previous reports [29-31]. Further, the

peak at 951 cm^{-1} was due to C-O stretching mode, that at 1011 cm^{-1} was due to symmetrical mode of W=O stretching mode, the sharp peak δ(H-O-H) bending vibration mode at 1623 cm^{-1} and γ(O-H) stretching mode at 3446 cm^{-1} were attributed to absorption of water molecule. When irradiation time increased, both the δ (H-O-H) bending vibration mode and γ (O-H) stretching mode gradually decreased.

3.2. Optical analysis

The optical properties of the samples were investigated by means of UV-Vis and photoluminescence technique analysis. **Figure 6** shows the UV absorption spectra of WO_3 samples. The UV absorption spectra obtained display a broad band with maximum at 343 nm, blue-shifted when compared with the bulk WO_3 material. The UV-VIS absorption spectra of semiconductor nanoparticles were size dependent, which is consequence of quantum confinement of the photo generated electron-hole pairs. Predominantly, wavelength at the maximum exciton absorption (λ_{max}) decreases as a result of decreasing of nanoparticles size. The decrement of particles size increases the optical bandgap energy of the nanoparticles, indicating the presence of quantum confinement effect, which is consistent with previous theoretical argument by Brus [32]. Increasing the irradiation time, the absorption band intensity gradually increased. The bandgap energies were calculated using the energy relation of 1242/λ and their estimated bandgap values were calculated to be around 3.62 eV.

Figure 7 shows the PL emission spectra, obtained at an excitation wavelength of 340 nm. A weak emission peak in the violet region at 400 nm was obtained in addition with a strong blue emission at 435 nm together with a small emission peak at 460 nm. This emission behavior is related to the transition/attribution due to the localized states of oxygen vacancy/surface states of conduction band. The observed results are similar to previous reports [33-34]. While irradiation time increased from 10 min to 30 min, the emission intensity gradually increased in the blue emission region (i.e. blue-shift) and gradually decreased in green emission region (i.e. red-shift). We believe that these observations are related to decrease of oxygen defect states.

3.3. Thermal-aging of as-synthetized WO_x samples

Preliminary electrical and sensing tests have shown that, in order to have measurable resistance values and reliable and stable sensing behavior, it is necessary to operate at temperatures higher than 250 °C. This is in according with the general behavior of metal oxide nanostructures for gas sensing applications [35]. In fact, to stabilize their very reactive surface, a thermal aging of metal oxides at a proper high temperature is generally performed.

Therefore, to acquire information about the thermal behavior of as-prepared samples, a TGA analysis has been carried out. TGA analysis of S30 sample is reported in **Figure 8**. The TGA result shows two step weights loss in this range of temperature. The first small weight loss of 3.4% was observed at 195 °C and second weight loss was observed at 532 °C, attributed to a possible loss of water absorbed during the synthesis and storage in the ambient. The total weight loss corresponded to the value of 7.0 wt.%, and this value is consistent with the starting phase composition as $WO_3 \cdot H_2O$ (theoretical crystallization water 7.20 wt. %).

Based on TGA indication, the as-synthesized samples were aged thermally in air at the temperature of 350 °C. The verification of the crystalline phase formed after thermal aging has been made by acquiring XRD patterns. The results of XRD analysis are shown in **Figure 9.** According to reports by other authors [36], we observed that monoclinic $WO_{2.9}$ phase has been converted into WO_3.

3.4. Gas sensing tests

The sensing properties of thermal-aged WO_x nanoparticles were investigated for the monitoring of ethanol in air. Before sensing tests the sensor was allowed to stabilized at 350 °C. During this step no remarkable modifications of the electrical characteristics have been noted. The fabricated WO_x sensors were tested from room temperature to 350 °C. However, at temperature lower than 250 °C, the sensors resistance is very high, so we cannot perform any measurement using our instrumentation. Above 250 °C, the resistance falls into a measurable range (**Figure 10**). The sensor response increases with the increasing of the

temperature, reaches a maximum at 300 °C and then decreases with further increasing the operating temperature.

Figures 11(a-c) show the responses of S10, S20 and S30 sensors to different concentrations of C_2H_5OH in the range of 10–400 ppm. It is clearly observed that when the sensor is exposed to ethanol vapor pulses under dynamic cycling, the resistance changes rapidly toward a new equilibrium value. Once the ethanol vapor was vented from the sensor chamber, the resistance returned to the baseline value, demonstrating the good reproducibility and reversibility of the sensor response.

All investigated sensors showed a decrease of resistance in the presence of ethanol. As ethanol is a reducing gas, this suggests that the WO_3 nanostructures behave as an n-type semiconductor [37]. Indeed, according the usual sensing mechanism for metal oxides, in the presence of oxygen in the surrounding environment, it is chemisorbed on the surface of the sensing layer as oxygen ion species. In particular, in the range of temperature 150 - 400 °C, $O^-_{(ads)}$ is the dominant typical oxygen adsorbed specie on metal oxides [38]. The reaction of ethanol with the chemisorbed reactive oxygen ions on the surface:

$$C_2H_5OH_{(g)} + 6\,O^-_{(ads)} \rightarrow 2\,CO_{2(g)} + 3\,H_2O_{(g)} + 6\,e^- \qquad (2)$$

produces electrons which are released into the WO_3 bulk, thereby increasing the electron carriers in the n-type semiconducting film. This in turn, increases the resistance of the sensing layer.

Figure 11d reports the calibration curves, extrapolated from the previous dynamic responses, for each sensor. As observed the sensor S10 shows the highest sensitivity suggesting that, the WO_x nanoparticles synthesized by the shorter irradiation time of 10 minutes is the most suitable as ethanol sensing material. From the log-log interpolation reported in the inset of **Figure 11d**, the limit of detection for sensor S10 has been estimated to be about 3 ppm at a signal to noise ratio on the intercept (S/N = 3).

Reproducibility and selectivity are other important characteristics for practical sensors. In particular, baseline and signal stability of sensors are of outmost importance

because allows minimal equipment checking and maintenance. **Figure 12a** shows the response curve of the S10 sensor towards three subsequent pulses of 100 ppm of ethanol at 300 °C. It appears clear that the response of the material is constant confirming the stability of the sensor material and signal reliability. At the optimum working temperature of 300 °C, the sensor shows also a fast response time as low as 10 s towards 100 ppm ethanol, however recovery time is more longer as 290 s (**Figure 12b**).

It is noteworthy to mention that the reproducibility tests have been carried out with the sensor S10 fabricated some months earlier. Furthermore, looking at the previous tests with this sensor (see **Figure 11b**) we can observe that both the baseline resistance and signal response to 100 ppm of ethanol have been maintained. These observations indicate that the synthesized material is stable and can be used as sensing layer for developing practical conductive gas sensors.

The sensing response of sensor S10 toward different reducing and oxidizing gases such as NO, NO_2, carbon monoxide, carbon dioxide, methane, ammonia and hydrogen at different concentrations were registered to evaluate the ethanol selectivity of the device against these gases. The values of the response of the sensor to these different gases are reported in **Figure 13.** Obviously, the results indicates that the sensing response towards ethanol is higher compared to that registered for the other gases, demonstrating its good selectivity to ethanol.

The good performances of the proposed sensor are compared to ones exhibited by other WO_3 sensor reported in the previous literature for ethanol monitoring in air (**Table 1**).

4. Conclusion

Tungsten oxide samples have been successfully synthesized via simple microwave irradiation method. The orthorhombic and monoclinic crystal structure were confirmed from

the XRD patterns. As-synthesized samples are constituted by irregular shaped particles containing also some well-structured rod shape particles. An enhanced optical absorption and emission behaviors were observed from the UV and PL results, respectively.

The sensing properties of as-prepared WO_3 nanoparticles towards ethanol were investigated. After thermal aging of the WO_3 nanoparticles at 350 °C, the sensors demonstrate good sensitivity to ethanol. The obtained results suggest that the as-prepared samples may be suitable, after a mild temperature treatment, for gas sensing applications.

References

1. J. Zhang, X.L. Wang, X.H. Xia, C.D. Gu, J.P. Tu, Electro chromic behavior of WO3 nano tree films prepared by hydrothermal oxidation, Solar Energy Materials and Solar Cells 95 (2011) 2107–2112.
2. K. A. Gesheva, T. M. Ivanova, G. Bodurov, Transition metal oxide films: technology and Smart Windows electro chromic device performance, Progress in Organic Coatings 74 (2012) 635–639.
3. N. Lu, X. Gao, C. Yang, F. Xiao, J. Wang, X. Su, Enhanced formic acid gas-sensing property of WO3 nanorod bundle via hydrothermal method, Sensors and Actuators B, 223, (2016) 743–749.
4. A. A. Dakhel, Investigations on Sn-doped Ni oxide thin films and their use as optical sensor devices, Journal of Non-Crystalline Solids 358 (2012) 285–289.
5. S. Yao, F. Qu, G. Wang, X. Wu, Facile hydrothermal synthesis of WO_3 nanorods for photocatalysts and supercapacitors, J. of Alloys and Compounds 724 (2017) 695-702.
6. T. Stubhan, N. Li, N. A. Luechinger, S. C. Halim, G. J. Matt, C. J. Brabec, High fill factor polymer solar cells incorporating a low temperature solution processed WO_3 hole extraction layer. Adv. Energy Mater, 2 (2012) 1433–1438.
7. C. Santato, M. Ulmann, J. Augustynski, Enhanced visible light conversion efficiency using nanocrystalline WO_3 films, Adv. Mater., 13 (2001) 511–514.
8. J. Wang, Z. Wang, C.-J. Liu, Enhanced activity for CO oxidation over WO_3 nanolamella supported Pt catalyst, ACS Appl. Mater. Interfaces, 6 (2014) 12860-12867.

9. M. Acosta Díaz, C. Vales Pinzón, I. Riech Méndez, WO3 thin films by sol–gel: structural and morphological properties, Engineering 13 (3) (2009) 29–38.
10. X. Lu, X. Liu, W. Zhang, C. Wang, Y. Wei, Large-scale synthesis of tungsten oxide nanofibers by electro spinning, Journal of Colloid and Interface Science 298 (2006) 996–999.
11. L. Xiong, T. He, Synthesis and characterization of ultrafine tungsten and tungsten oxide nanoparticles by a reverse micro emulsion-mediated method, *C*hem. Mater., 2006, 18 , 2211–2218.
12. S. Supothina, P. Seeharaj, S. Yoriya, M. Sriyudthsak, Synthesis of tungsten oxide nanoparticles by acid precipitation method, Ceramics International 33 (2007) 931–936.
13. Y.-G. Choi, G. Sakai, K. Shimanoe, N. Miura, N. Yamazoe, Preparation of aqueous sols of tungsten oxide dihydrate from sodium tungstate by an ion-exchange method, Sensors and Actuators B 87 (2002) 63–72.
14. A. Mirzaei, G. Neri, Microwave-assisted synthesis of metal oxide nanostructures for gas sensing application: A review, Sensors and Actuators B: 237, (2016) 749-775.
15. Q. Sun, J. Luo, Z. Xie, J. Wang, X. Su, Synthesis of monodisperse $WO_3.2H_2O$ nanospheres by microwave hydrothermal process with L (+) tartaric acid as a protective agent, Materials Letters 62 (2008) 2992–2994.
16. N. Le Houx, G. Pourroy, F. Camerel, M. Comet, D. Spitzer, WO3 nanoparticles in the 5–30 nm range by solvothermal synthesis under microwave or resistive heating, The Journal of Physical Chemistry C 114 (2010) 155–161.
17. J. Sungpanich, T. Thongtem, S. Thongtem, Large-scale synthesis of WO3 nanoplates by a microwave-hydrothermal method, Ceramics International 38 (2012) 1051–105.
18. Phuruangrat, D. J. Ham, S. J. Hong, S. Thongtem and J. S. Lee, Synthesis of hexagonal WO_3 nanowires by microwave-assisted hydrothermal method and their electro catalytic activities for hydrogen evolution reaction J. Mater. Chem., 2010, 20, 1683–1690
19. D. B. Hernandez-Uresti, D. Sanchez Martinez, A. Martinez-de la Cruz, S. Sepúlveda-Guzmán, Leticia M. Torres-Martinez, Characterization and photocatalytic properties of hexagonal and monoclinic WO_3 prepared via microwave-assisted hydrothermal synthesis, Ceramics International 40 (2014) 4767–4775.
20. N. Le Houx, G. Pourroy, F. Camerel, M. Comet and D. Spitzer, WO3 Nanoparticles in the 5−30 nm Range by Solvothermal Synthesis under Microwave or Resistive Heating J. Phys. Chem. C, 2010, 114, 155–161.

21. K.-Hsin Chang, C.-Chang Hu, C.-Ming Huang, Y.-Ling Liu, C.-I. Chang, Microwave-assisted hydrothermal synthesis of crystalline WO_3–$WO_3 \cdot 0.5H_2O$ mixtures for pseudo capacitors of the asymmetric type Journal of Power Sources 196 (2011) 2387–2392.
22. G..Korotcenkov, Metal Oxides for Solid-State Gas Sensors: What Determines Our Choice? Mater. Sci. Eng., B 2007, 139 (1), 1−23.
23. N. Lavanya, A.C. Anithaa, C. Sekar, K. Asokan, A. Bonavita, N. Donato, S. G. Leonardi, G. Neri, Effect of gamma irradiation on structural, electrical and gas sensing properties of tungsten oxide nanoparticles, Journal of Alloys and Compounds 693, 366-372.
24. G. Neri, G. Micali, A. Bonavita, S. Ipsale, G. Rizzo, M. Niederberger, N. Pinna, Tungsten oxide nanowires-based ammonia gas sensors, Sensor Letters 6, 590-595.
25. M. Z. Ahmad, J.H. Kang, A.Z. Sadek, A. Moafi, G. Sberveglieri, W. Wlodarski, Synthesis of WO_3 nanorod based thin films for ethanol and H_2 Sensing. Procedia Eng. 47 (2012) 358–361.
26. X. Su, Y. Li, J. Jian, J. Wang, In situ etching WO_3 nanoplates: Hydrothermal synthesis, photoluminescence and gas sensor properties, Materials Research Bulletin 45 (2010) 1960–1963.
27. A.Yu. Lyashkov, A.S. Tonkoshkur, V.O. Makarov, Gas sensing properties of WO_3-based ceramics to ethanol vapors, Sensors and Actuators B 148 (2010) 1–5.
28. A. Mirzaei, S. G. Leonardi, G. Neri, Detection of hazardous volatile organic compounds (VOCs) by metal oxide nanostructures-based gas sensors: A review, Ceramics International 42, 2016, 15119-15141.
29. H.-F. Pang, X. Xiang, Z.-J. Li, Y.-Q. Fu, X.-T. Zu, Hydrothermal synthesis and optical properties of hexagonal tungsten oxide nanocrystals assisted by ammonium tartrate, Phys. Status Solidi A, 209 (2012) 537–544.
30. P. Porkodi, V. Yegnaraman, D. Jeyakumar, Polyol mediated synthesis of tungsten trioxide and Ti doped tungsten trioxide. Materials Research Bulletin, 41 (2006), 1476-1486.
31. M. Deepa, N. Sharma, P. Varshney, S. P.Varma, S. A. Agnihotry, FTIR investigations of solid precursor materials for sol-gel deposition of WO_3 based electrochromic films J. of Materials Science 35 (2000) 5313 – 5318.
32. L.E. Brus,. Electron-electron and electron hole interactions in small semiconductor crystallites: The size dependence of the lowest excited electronic state. J. Chem. Phys., 80 (1984) 4403.

33. M. A. Gondal, A. Bagabas, A. Dastageer, A. Khalil, Synthesis, characterization, and antimicrobial application of nano-palladium-doped nano-WO_3, Journal of Molecular Catalysis A: Chemical 323 (2010) 78–83.
34. S. Park, H. Kim, C. Jin, C. Lee, Intense ultraviolet emission from needle-like WO_3 nanostructures synthesized by noncatalytic thermal evaporation, Nanoscale Research Letters 6 (2011) 45.
35. Neri, G. First Fifty Years of Chemoresistive Gas Sensors. Chemosensors 3 (2015) 1-20.
36. S. Masoomeh, A. Novinrooz, H. Noorkojouri. Preparation and characterization of WO3 electrochromic films obtained by the sol-gel process. Iranian J. of Chemistry and Chemical Engineering 25 (2006) 25-29.
37. X.-Lin Li, T.-Jun Lou, X.-Ming Sun, and Ya-Dong Li, Highly Sensitive WO_3 Hollow-Sphere Gas Sensors, Inorganic Chemistry, 43 (2004) 5442-5449.
38. N. Barsan, U. Weimar, Conduction model of metal oxide gas sensors, J Electroceramics, 7 (2001) 143–167.
39. C. Song, C. Li, Y. Yin, J. Xiao, X. Zhang, M. Song, W. Dong, Preparation and gas sensing properties of partially broken WO_3 nanotubes, Vacuum 114 (2015) 13-16.
40. X. Chang, Q. Zhou, S. Sun, C. Shao, Y. Lei, T. Liu, L. Dong, Y. Yin, Graphene-tungsten oxide nanocomposites with highly enhanced gas-sensing performance, J Alloys Compd, 705 (2017) 659-667.
41. M. Ahsan, M. Z.Ahmad, T. Tesfamichael J. Bell, W. Wlodarski, N. Motta, Low temperature response of nanostructured tungsten oxide thin films toward hydrogen and ethanol, Sens. Actuators B: Chemical 173 (2012) 789-796.
42. W. Zeng, B. Miao, T. Li, H. Zhang, S. Hussain, Y. Li, W. Yu, Hydrothermal synthesis, characterization of h-WO_3 nanowires and gas sensing of thin film sensor based on this powder, Thin Solid Films 584 (2015) 294–299.
43. X. Li, G. Zhang, F. Cheng, B. Guo, J. Chen, Synthesis, characterization, and gas-sensor application of WO3 nanocuboids, J Electrochem Soc, 153 (2006) 133-137.

44. J. Xiao, C. Song, W. Dong, C. Li, Y. Yin, X. Zhang, M. Song, Synthesis, Characterization, and Gas Sensing Applications of WO_3 Nanobricks, J Mater Eng Perform, 24 (2015) 3026-3031.

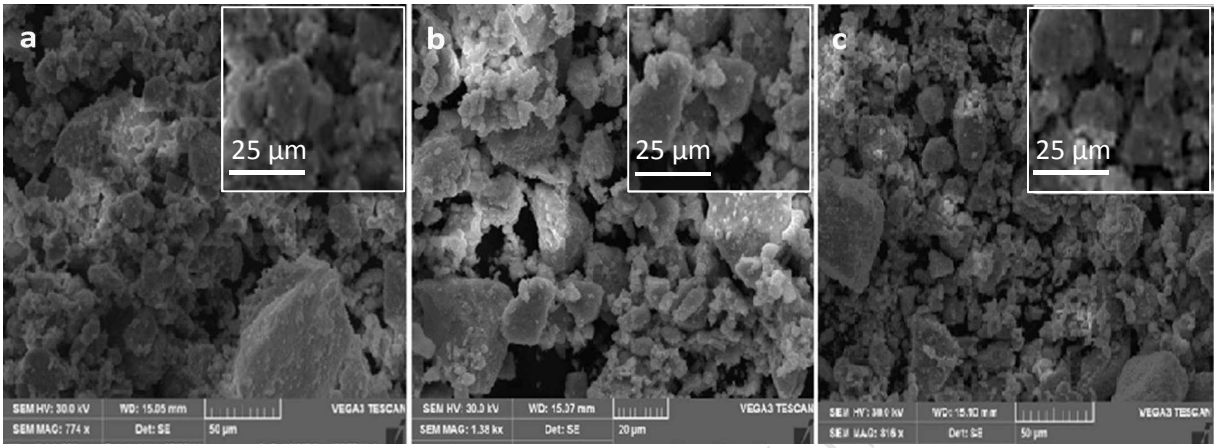

Figure 1. SEM images of WO_3 samples (a) S10, (b) S20 and (c) S30.

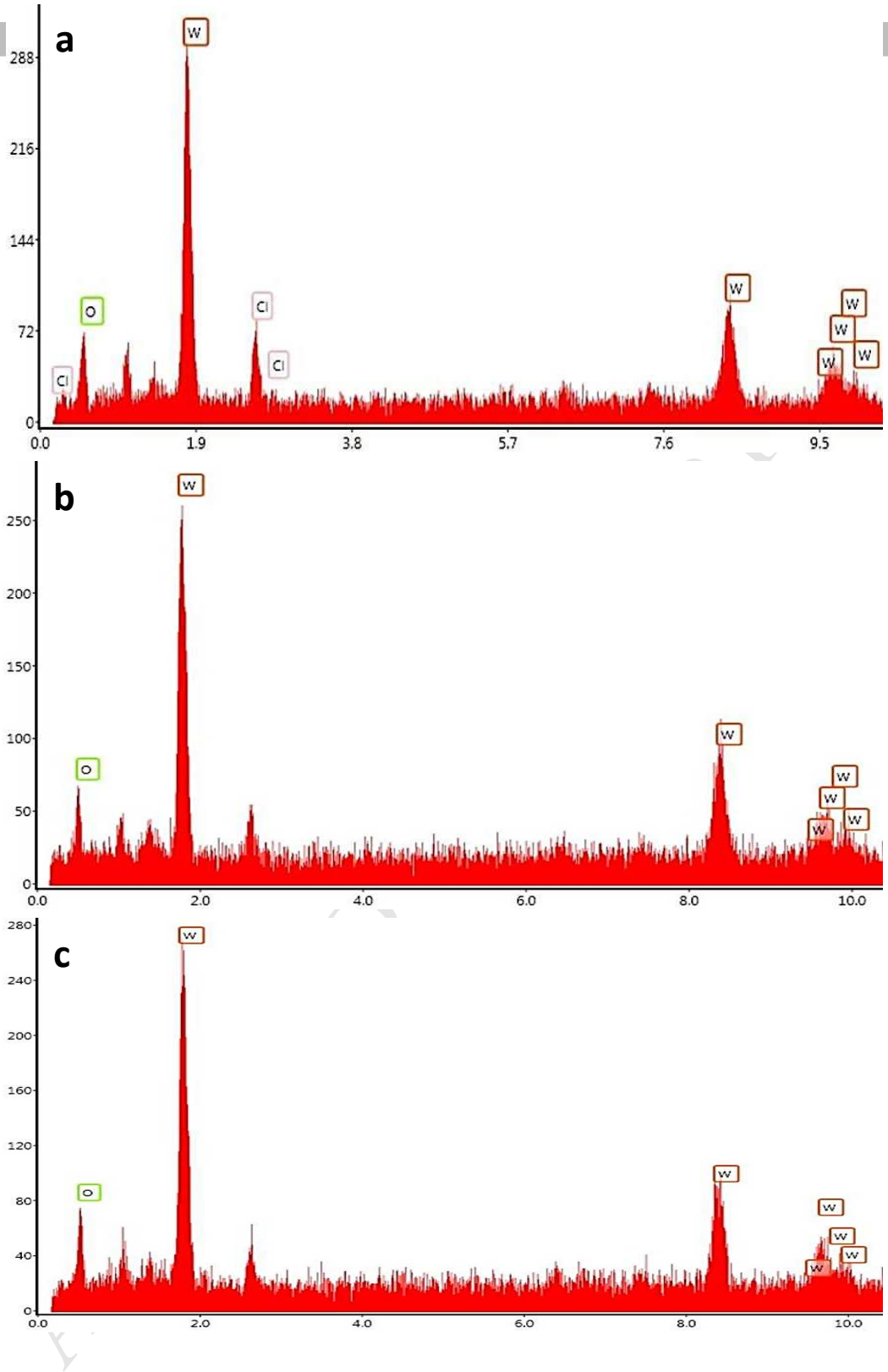

Figure 2. EDAX spectra of WO_3 samples (a) S10, (b) S20 and (c) S30.

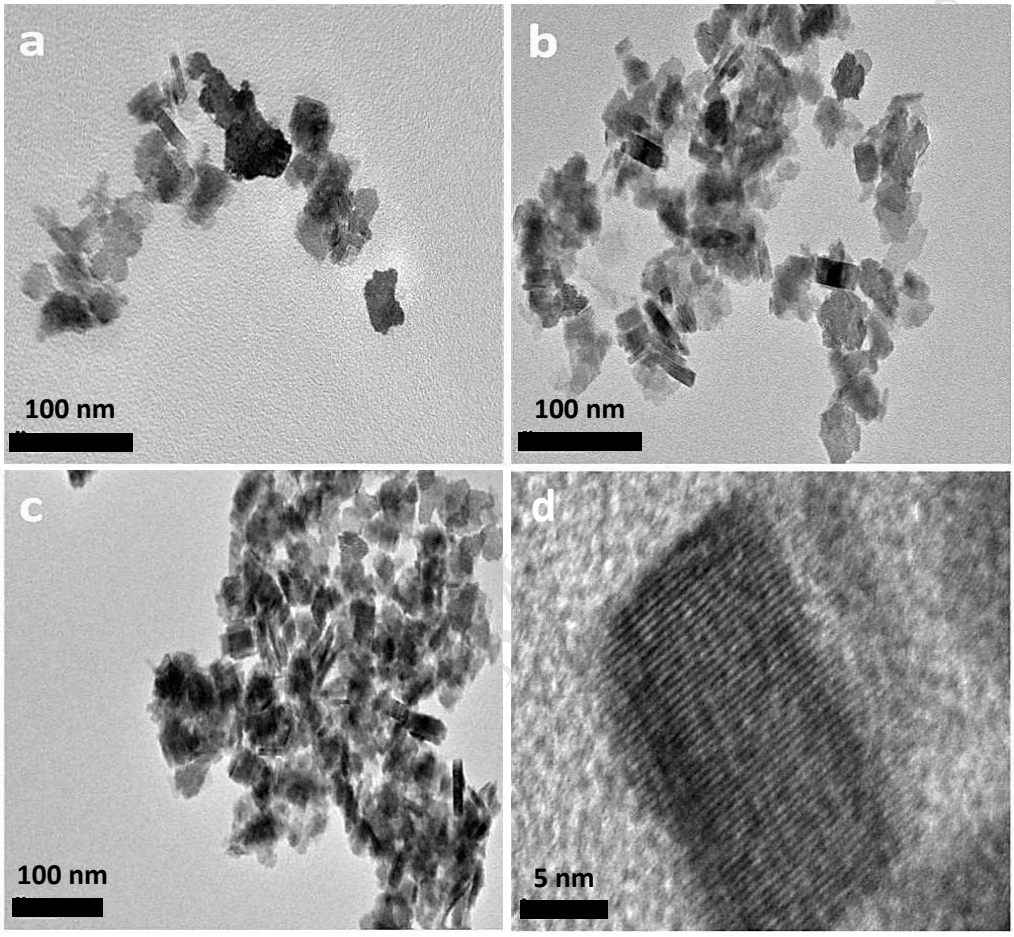

Figure 3. TEM images of WO_3 samples (a) S10, (b) S20 and (c) S30. HRTEM image of one rod-like particle (sample S30).

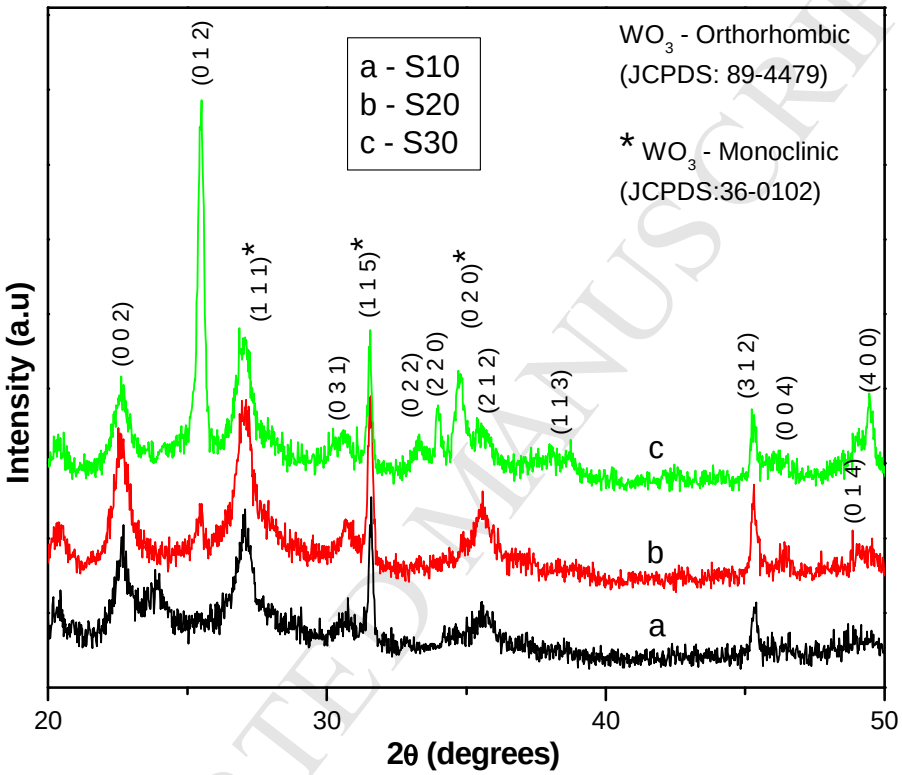

Figure 4. XRD patterns of WO_3 samples (a) S10, (b) S20 and (c) S30.

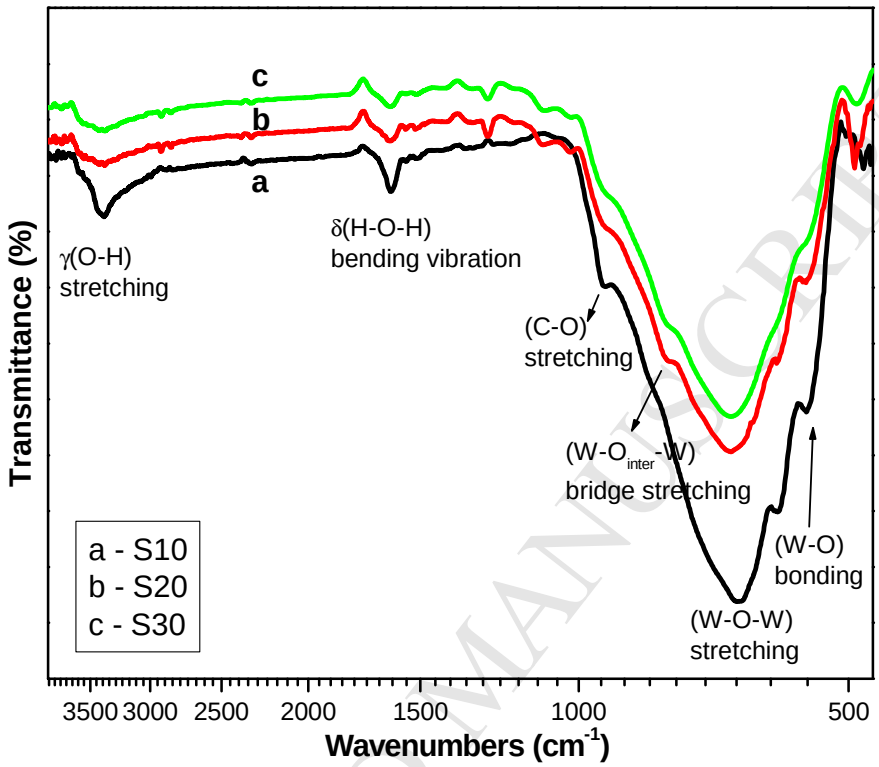

Figure 5. FTIR spectra of WO_3 samples (a) S10, (b) S20 and (c) S30.

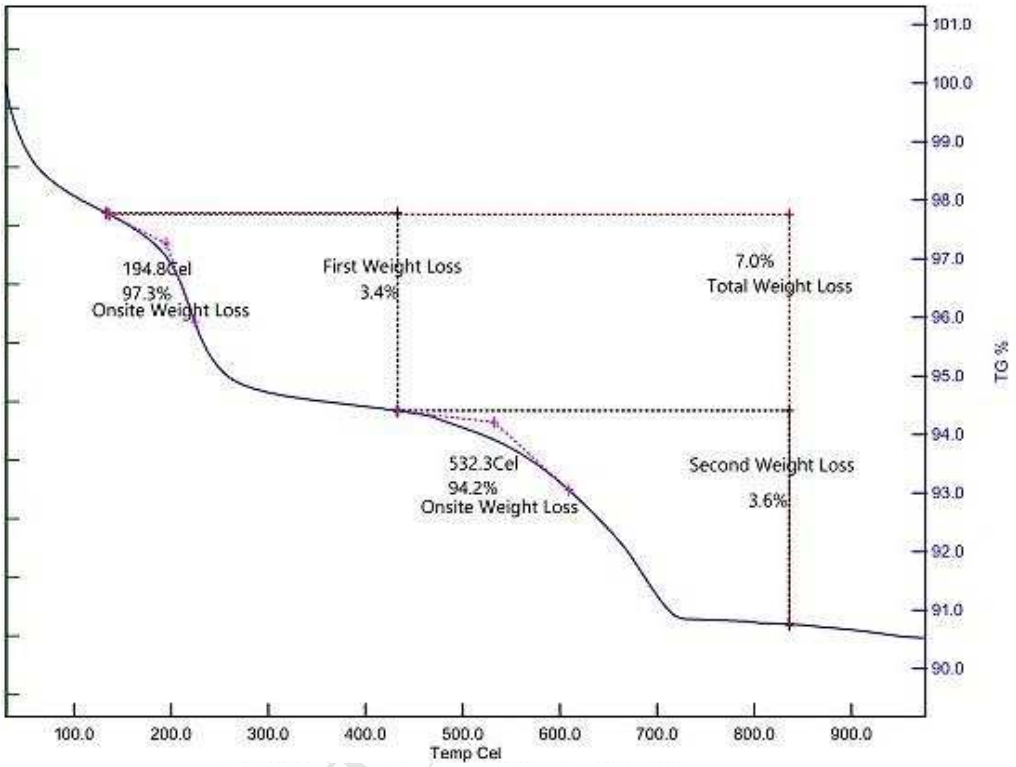

Figure 6. TGA of WO_3 nanoparticles. Sample S30.

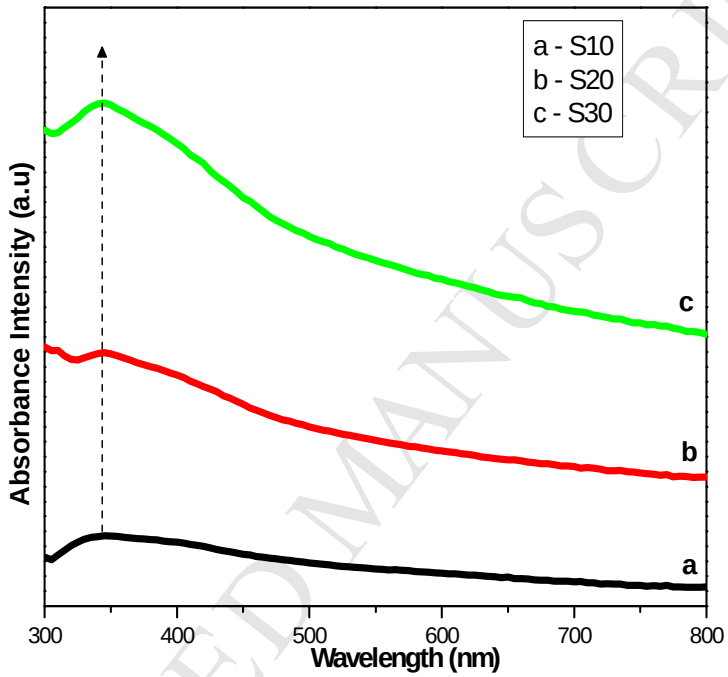

Figure 7. UV spectra of WO_3 samples (a) S10, (b) S20 and (c) S30.

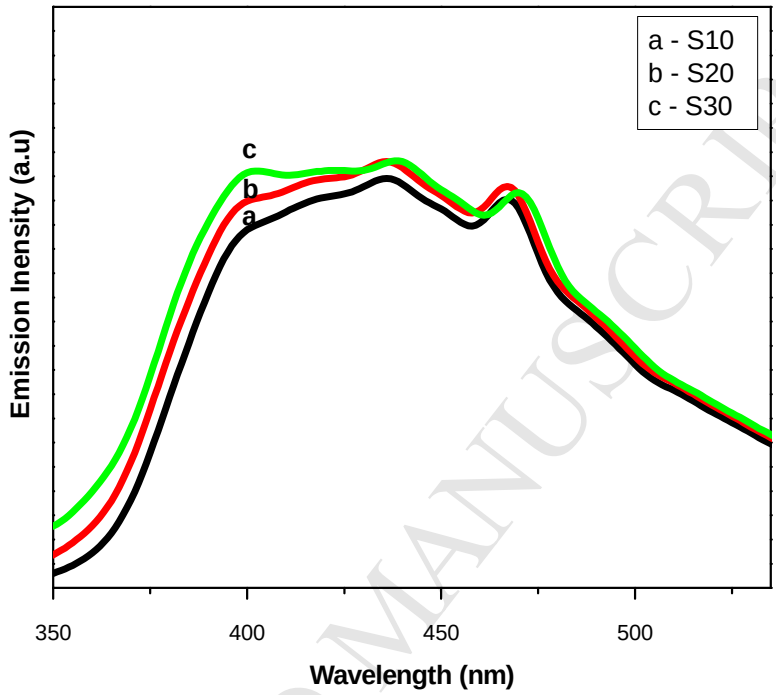

Figure 8. PL emission spectra of WO_3 samples (a) S10, (b) S20 and (c) S30.

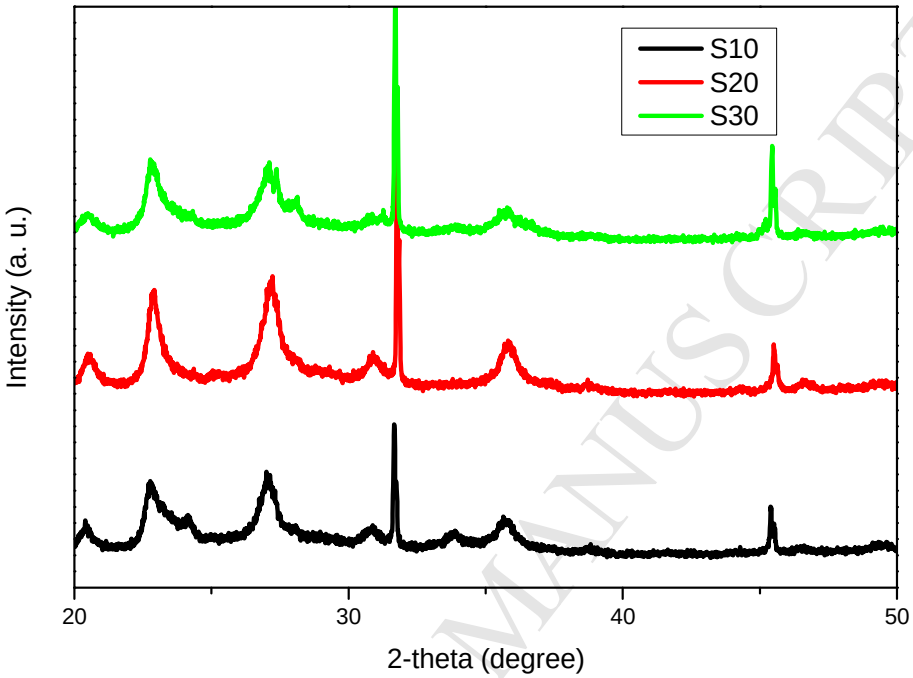

Figure 9. XRD pattern of samples (a) S10, (b) S20 and (c) S30 after annealing at 350 ºC for 2 hours.

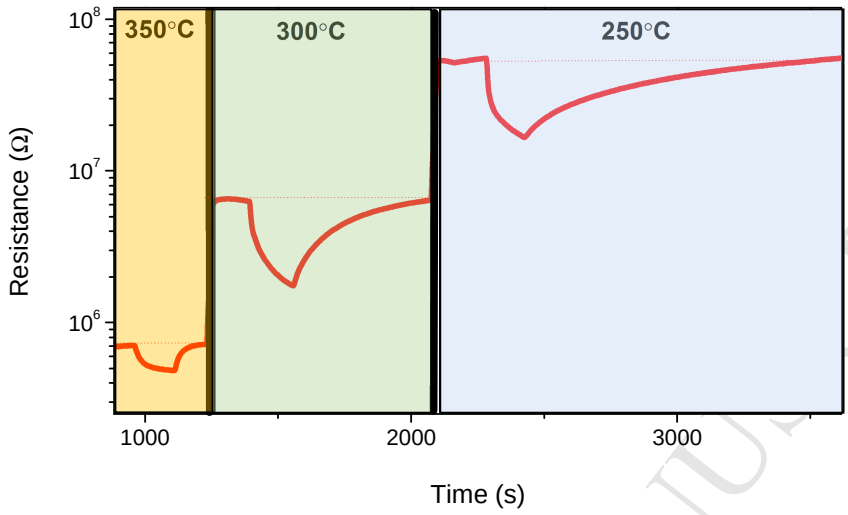

Figure 10. Response of sensor S20 after annealing at 350 ºC for 2 hours toward 50 ppm EtOH.

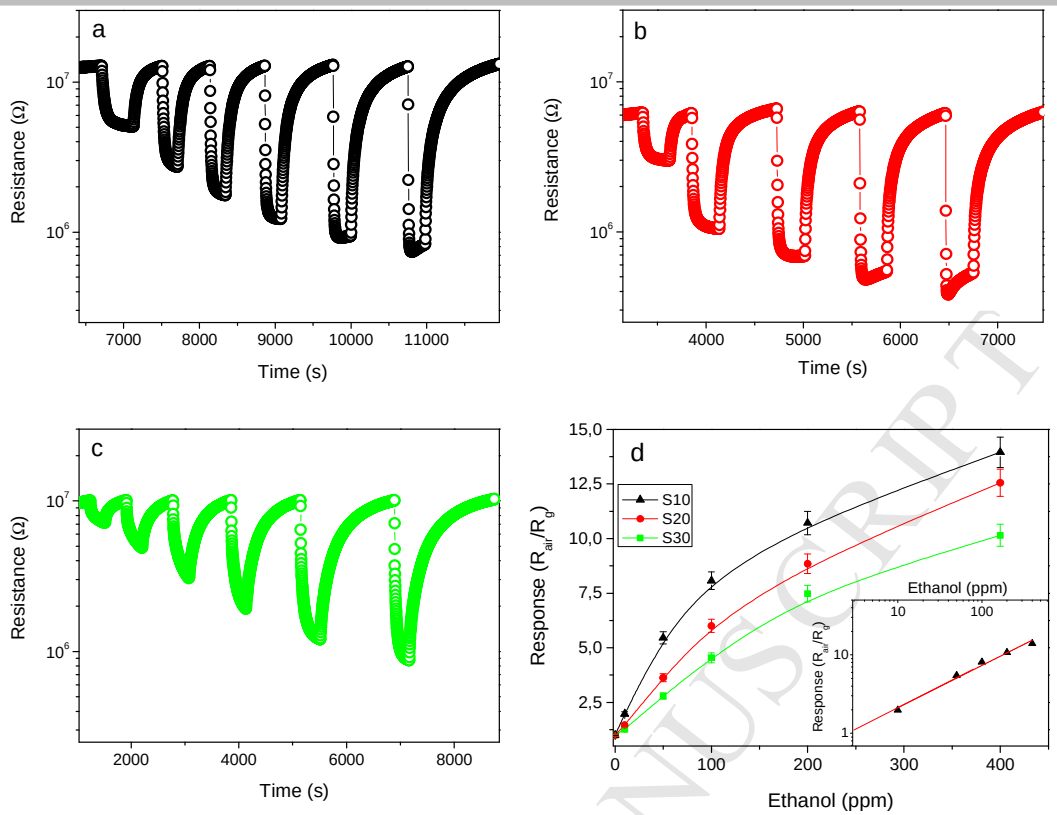

Figure 11. Response of a) S10 b) S20 c) S30 after annealing at 350 ºC for 2 hours toward different concentrations of EtOH at operating temperature of 300 ºC. d) Corresponding calibration curves for S10, S20 and S30.

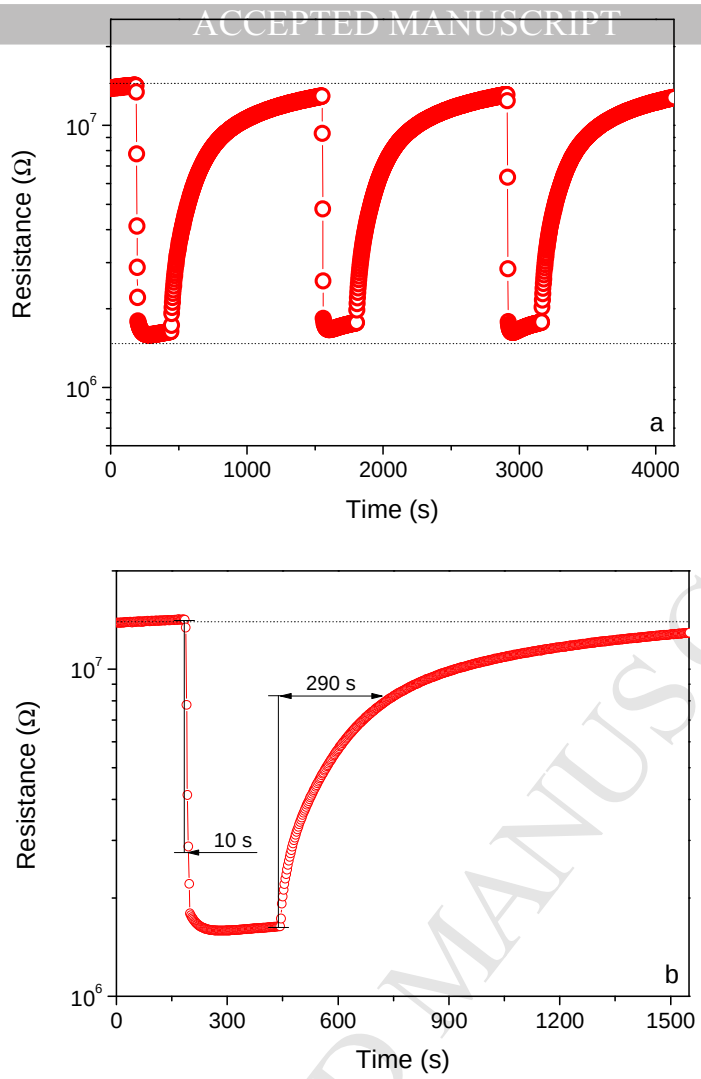

Figure 12. a) Dynamic response curve of the S10 sensor towards subsequent pulses of 100 ppm of ethanol at 300 °C; b) response and recovery times.

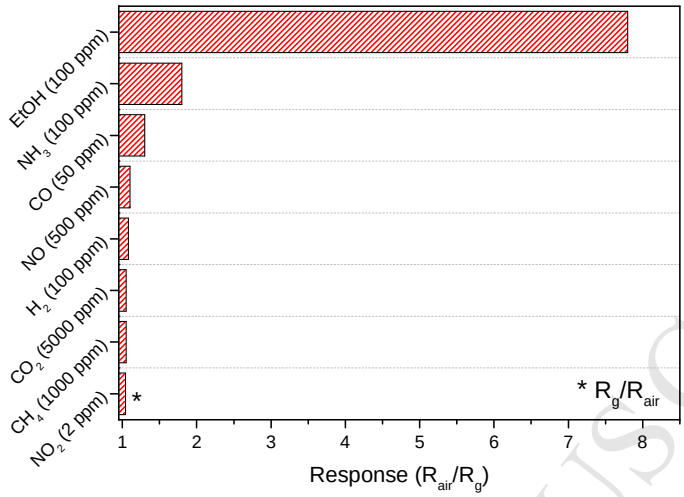

Figure 13. Response of sensor S10 toward different reducing and oxidizing gases at the operating temperature of 300 ºC.

Table 1. Comparison of ethanol sensing properties of different tungsten oxide nanostructures in the literatures.

Sensing Material	*Synthesis method*	*Conc.(ppm)*	*Response (R_a/R_g)*	*Response/Recovery times (s)*	*Operating Temp.(°C)*	*Ref.*
WO_3 nanotube	Solvothermal	100	3.5	1/9	340	[39]
$W_{18}O_{49}$/graphene	Solvothermal	500	5.2	6/8	300	[40]
WO_3 film	Thermal evaporation	185	1.3	180/288	150	[41]
WO_3 nanowires	Hydrothermal	100	22	6/8	300	[42]
WO_3 nanocuboids	Hydrothermal	1000	9.2	21/23	300	[43]
WO_3 nanobricks	Hydrothermal	100	6.5	3/11	300	[44]
WO_3 nanopowders	Hydrothermal	100	8.5	10/290	300	This work

Highligths

- WOx NPs are synthesized by MW-hydrothermal method without needs of surfactants.
- The effect of MW irradiation time on WOx NPs properties was investigated.
- A conductometric WOx ethanol sensor has been fabricated.
- WOx NPs-based sensor showed high performance for ethanol sensing.